Direct quantification of electrochemical CO_2 reduction products with an improved DEMS setup

van den Berg, Daniël; Lopuhaä, Hendrik Paul; Kortlever, Ruud

DOI
10.1016/j.checat.2024.101065

Publication date
2024

Document Version
Final published version

Published in
Chem Catalysis

Citation (APA)
van den Berg, D., Lopuhaä, H. P., & Kortlever, R. (2024). Direct quantification of electrochemical CO_2 reduction products with an improved DEMS setup. *Chem Catalysis*, *4*(8), Article 101065. https://doi.org/10.1016/j.checat.2024.101065

Important note
To cite this publication, please use the final published version (if applicable).
Please check the document version above.

Chem Catalysis

CellPress
OPEN ACCESS

Resource

Direct quantification of electrochemical CO_2 reduction products with an improved DEMS setup

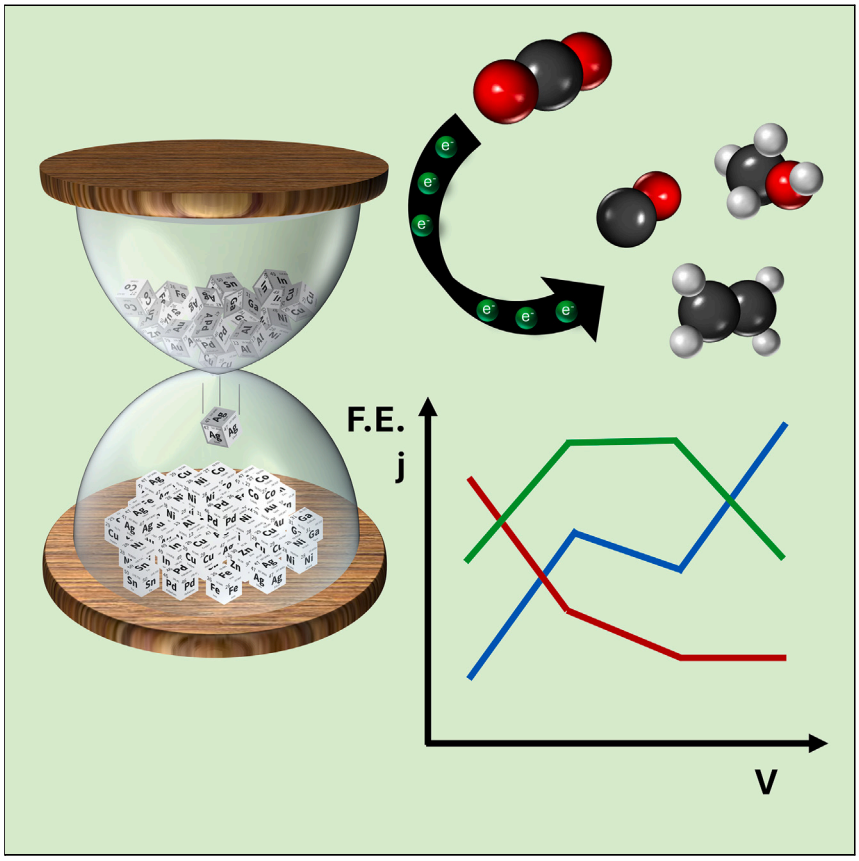

The CO_2 reduction reaction (CO_2RR) is a promising route for converting waste CO_2 into valuable chemicals and fuels. The analytical tools to quantify CO_2RR products are often slow and have high limits of detection, effectively slowing down research. We report a differential electrochemical mass spectrometry (DEMS) setup capable of directly quantifying CO_2RR products in the gaseous and liquid phases. We discuss the design choices, specifically regarding the mass transfer rate of CO_2, and the quantification of CO_2RR products.

Daniël van den Berg, Hendrik Paul Lopuhaä, Ruud Kortlever

r.kortlever@tudelft.nl

Highlights

We design a DEMS that enables swift quantification of products from CO_2 reduction

First setup able to simultaneously quantify carbon monoxide and liquid products

Validation by performing measurements with polycrystalline Cu and Ag

van den Berg et al., Chem Catalysis 4, 101065 August 15, 2024
https://doi.org/10.1016/j.checat.2024.101065

Chem Catalysis

CellPress
OPEN ACCESS

Resource

Direct quantification of electrochemical CO_2 reduction products with an improved DEMS setup

Daniël van den Berg,[1] Hendrik Paul Lopuhaä,[2] and Ruud Kortlever[1,3,*]

SUMMARY

The analytical tools to quantify CO_2RR products are often slow and have high limits of detection. As a result, researchers are forced to extend the duration of their experiments to accumulate sufficient product and surpass these detection limits. This slows down research considerably, and the research scope often remains limited. To help speed up CO_2RR catalyst studies, we have developed a new differential electrochemical mass spectrometer (DEMS) setup and cell design that enables the quantification of major gaseous and liquid products significantly faster than conventional analytical techniques. Special attention was given to the hydrodynamics of the cell to avoid mass transfer limitations and the calibration of the setup to accurately quantify the major CO_2 reduction products. As proof of concept of the methodology, the products formed during CO_2RR on a polycrystalline Ag and Cu electrode in a 0.1-M $KHCO_3$ electrolyte at different potentials were measured and quantified.

INTRODUCTION

The electrochemical CO_2 reduction reaction (CO_2RR) toward valuable products using renewable electricity can offer an efficient route to reduce CO_2 emissions and the dependence on fossil resources.[1–3] However, a stable and selective catalyst for the direct conversion of CO_2 toward these valuable products has yet to be found. Depending on the catalyst, different gaseous and liquid products are produced on the cathode. During initial catalyst development studies, researchers generally use in-line gas chromatography (GC) and offline high-performance liquid chromatography (HPLC) or NMR spectroscopy to quantify gaseous and liquid products, respectively.[4] However, these analytic techniques have long analyses times and relatively high limits of detection, forcing researchers to extend the duration of experiments to accumulate a detectable concentration of products. Furthermore, HPLC and NMR measurements are offline and indirect, making it difficult to keep track of time-dependent processes such as reaction kinetics or catalyst stability. Therefore, considerable effort has been made to develop techniques that are able to quantify the production rates of major CO_2RR products directly and in real time. Differential electrochemical mass spectrometry (DEMS) uses a pervaporation membrane to separate (dissolved) gases and volatile organic compounds from the electrolyte. The production rates of both gaseous and liquid products are quantified by monitoring the responses of the products' mass peaks in the mass spectrum. Since MS has a lower limit of detection and both liquid and gaseous products are measured directly in the same setup, development of new CO_2RR catalysts can be sped up significantly.

One of the earliest DEMS setups that was applied for the reduction of CO_2 was used to monitor the adsorption of CO on Pt.[5] Wolter and Heitbaum placed a thin, porous

THE BIGGER PICTURE

To successfully transition from a fossil fuel-based society to one based on renewable energy, switching only to renewable energy sources is not enough. New, renewable processes and catalyst materials to synthesize bulk chemicals and transportation fuels will need to be developed. Electrochemical CO_2 reduction is a promising renewable process as it directly uses renewable energy to produce the desired chemicals under mild conditions.

Despite many efforts to find better catalytic materials, progress remains slow due to product quantification methods with high detection limits. In an effort to accelerate catalyst development research, we have designed an improved DEMS setup that is four times faster than conventional research in H cells. To the best of our knowledge, it is the first DEMS setup that is able to simultaneously quantify carbon monoxide and liquid products without the need for additional measurements.

Teflon membrane close to the working electrode inside the cell.[6] The setup allows for the detection and quantification of gaseous and dissolved molecules in the electrolyte. However, by placing the membrane close to the electrode's surface, reactants are removed from the electrolyte alongside the products, affecting the reaction conditions near the surface. Kita et al. developed another configuration that uses a small tip close to the electrode surface to remove formed products,[7] thereby inspiring later similar setups by Jambunathan and Hillier[8] and by Wonders et al.[9] These setups are able to detect a wide range of gaseous and volatile products, including hydrocarbons from electrochemical CO_2 reduction, CO_2 from CO adlayer oxidation, reduction and oxidation of acetylene, methanol oxidation, and NO and N_2O from hydroxylamine electrochemistry. However, it is difficult to quantify these measurements as the placement of the tip relative to the electrode surface is poorly controlled and leads to reproducibility issues. Recently, Clark et al. developed two setups that were able to semi-quantitatively monitor the production of formed alcohols during electrochemical CO_2 reduction. By deconvoluting the contribution of different species to the mass peaks, they were able to quantitatively determine the production rate of ethanol and 1-propanol on Cu.[10,11] However, the setup has several downsides. First, the cell requires a restrictive working electrode design, where the catalyst is either coated on the polytetrafluoroethylene (PTFE) membrane itself or has a specific ring-like geometry. Second, once the solubility limit of gaseous products in the electrolyte is reached and bubbles start to form, large SDs are encountered in both the current and mass signal response. Lastly, full deconvolution of the mass spectrum is not possible without separate measurements from a separate flow cell setup and additional HPLC measurements. While for ethanol oxidation DEMS setups for product quantification already exist,[12,13] all of the examples above are not able to rapidly quantify the product spectrum of previously untested catalyst material for CO_2RR products. Therefore, here, we set out to develop a DEMS setup capable of directly quantifying major CO_2RR products in both the gaseous and liquid phases in real time without any prior knowledge of the catalyst's product distribution. We discuss the design choices of a newly developed electrochemical cell and MS setup, specifically regarding the mass transfer rate of CO_2 to the electrode and the quantification of the CO_2RR products. Finally, we devise a numerical model to deconvolute the obtained mass peaks and quantify the production rates of the major CO_2RR products without the need for additional measurements. We show that with the help of this setup, we can determine the product spectrum as a function of applied potential in a much shorter timescale than is currently possible. This setup can thus enable the rapid screening of different catalyst materials, thereby speeding up catalyst development and facilitate testing catalyst under different process conditions.

RESULTS AND DISCUSSION

Cell design

An enlarged view of the cell is shown in Figure 1. The catholyte enters the cell through the side of the catholyte endplate (f), where it encounters the tip of the reference electrode (BASI RE-6) (g). From here, the electrolyte takes a sharp 90° turn and enters the flow plate (c). Here, the electrolyte flows through 10 parallel channels over the working electrode. Parallel channels are chosen to increase the flow velocity of the electrolyte through the channel, enhancing the mass transfer inside the cell. One side of the channel is exposed to the working electrode, while the other is in contact with the membrane (e.g., Nafion 117) to prevent product crossover to the counter electrode. At the end of the channel, the electrolyte flows back to the endplate and takes another sharp turn before exiting the cell. The same design is

[1]Large-Scale Energy Storage, Process, and Energy Department, Faculty of Mechanical Engineering, Delft University of Technology, Leeghwaterstraat 39, 2628 CB Delft, the Netherlands

[2]Statistics, Delft Institute of Applied Mathematics (DIAM), Electrical Engineering, Mathematics, and Computer Science, Delft University of Technology, Mekelweg 42628 CD Delft, the Netherlands

[3]Lead contact

*Correspondence: r.kortlever@tudelft.nl

https://doi.org/10.1016/j.checat.2024.101065

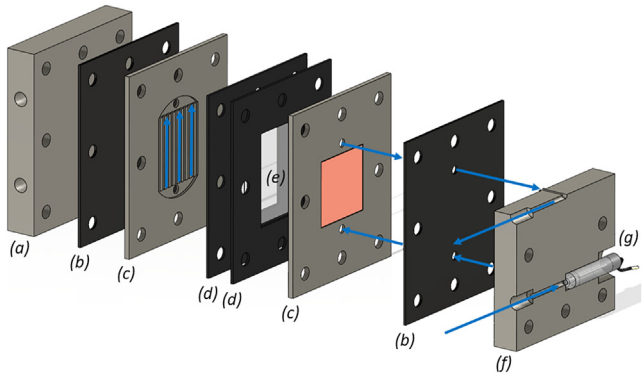

Figure 1. Magnified view of the DEMS cell

Each of the components is labeled accordingly: counter electrode endplate (a), silicon gasket (b), flow plate (c), membrane gasket (d), cationic membrane (Nafion 117) (e), catholyte endplate (f), and BASi RE-6 reference electrode (g).

maintained on the anodic side. The working and counter electrodes are placed parallel to each other to ensure a uniform potential distribution. The exposed surface areas of the working and counter electrodes are 2.75 cm^2 each. The flow- and endplates are manufactured from PEEK and are separated by silicon (0.015-in. high-temperature silicone rubber sheets, McMaster-Carr) gaskets to ensure leak tightness.

Cell mass transfer

When the conversion rate of CO_2 at the electrode becomes higher than the supply rate, the concentration of CO_2 at the electrode surface drops. A lower CO_2 concentration at the electrode surface affects the local reaction conditions and gives skewed results for the catalyst activity and selectivity. Therefore, CO_2 depletion at the surface due to mass transfer limitations should be prevented. Additionally, improved mass transfer conditions aid in product removal and hinder bubble formation. The mass transfer of CO_2 can be improved by increasing the flow rate of electrolyte through the cell, thereby decreasing the thickness of the diffusion boundary layer. However, the liquid product concentration also decreases at higher flow rates and could drop below the limit of detection of the MS. Therefore, the flow rate was varied to determine the optimal trade-off for product detection and the hydrodynamics of the cell.

The hydrodynamics of the new cell were determined using the ferri-/ferrocyanide redox system.[14] Since both redox systems use an aqueous electrolyte under the same temperature and flow rates, the governing hydrodynamics in both systems were considered to be the same. Therefore, any derived equations to describe the hydrodynamics in one system could be applied to the other by plugging in the corresponding values. The ferri-/ferrocyanide system is less complex than the CO_2RR system since it only has a single electron transfer and one reaction product. Linear sweep voltammograms were recorded at increasing electrolyte flow rates ranging between 0.2 and 5 mL/min Figure 2A shows that the limiting current goes up with electrolyte flow rate through the channels, as expected. An expression for the mass transfer of CO_2 to the electrode surface was derived using the film model (see section S.1 of the supplemental information). A Sherwood expression was obtained from van Male et al. for flow in a microchannel.[15] Using this expression, limiting currents from the model were calculated and compared with the experimentally obtained values in Figure 2A. As shown in Figure 2B, the experimental data fit well with the obtained expression for the Sherwood number. Therefore, the Sherwood expression can be used to calculate the concentration of CO_2 at the interface

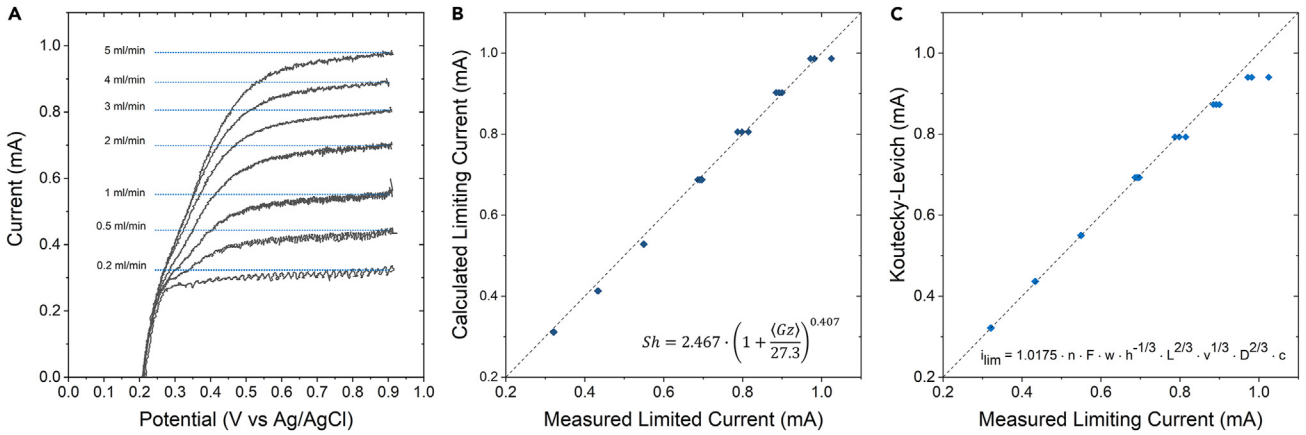

Figure 2. Hydrodynamics of the DEMS cell

(A) Linear sweep voltammograms with a sweep rate of 1 mV/s on glassy carbon in the DEMS setup using 0.1 M $KHCO_3$ + 5 mM $K_3Fe(CN)_6 \cdot H2O$ + 5 mM $K_4Fe(CN)_6$. Anodic limiting currents are obtained for each flow rate (dashed lines show the flow rates maintained through the cell).

(B and C) The experimentally measured limiting currents are set out against the calculated limiting currents from the Sherwood model (B) and Koutecký-Levich equation (C), respectively.

for a given flow rate and partial current densities during an experiment. Alternatively, the dependence upon the flow rate can be estimated using the Koutecký-Levich equation for channel electrodes that was derived by Scherson et al.[16]:

$$i_{lim} = 1.0175 \cdot n \cdot F \cdot w \cdot h^{-1/3} \cdot L^{2/3} \cdot v^{1/3} \cdot D^{2/3} \cdot c \qquad \text{(Equation 1)}$$

Here, n is the number of electrons that is transferred, F is the Faraday constant, w stands for the width of the channel, h is the half-height of the channel, L represents the length of the channel, v is the fluid flow velocity in the center of the channel, D is the diffusion coefficient, and c is the bulk concentration of the reacting species. Figure 2C shows that the experimentally obtained values also fit well with the Koutecký-Levich equation. Section S.2 of the supplemental information provides more details about how the limiting currents were calculated using these two models. According to Equation 1, the limiting current scales with the flow rate to the power of 1/3. This means that even though there is some initial gain from increasing the flow rate, the gain in mass transport to the surface is limited at higher flow rates. Therefore, the flow rate was set at 1 mL/min for all quantification measurements. The liquid phase product detection limit is ~5 μM at this flow rate according to Clark et al.[11] The limiting current density at this flow rate is 5.2 mA/cm^2 for 2 e^-/mol_{CO_2} such as CO and formate and 15.5 mA/cm^2 for 6 e^-/mol_{CO_2} products, such as ethylene and ethanol, as calculated by Equation 1. These limiting currents are on par with limiting current densities of other electrochemical cells in the literature.[17,18]

Reproducible collection efficiency

A schematic overview of the setup is given in Figure 3. During an experiment, electrolyte is stored in a reservoir and pumped through the cell by a peristaltic pump (Masterflex L/S Digital Miniflex Pump, Dual-Channel) lined with Precision Pump Tubing (Versilon 2001 Tubing, L/S 13). The electrolyte is pumped through the cell using positive pressure, as otherwise the liquid flow rate would become irregular when bubbles start to form. This is due to the fixed volume per minute that the peristaltic pump transports. Therefore, if the electrolyte is pumped using a negative pressure, then the pump has to transport both gas and liquid, and the volume amount of electrolyte will not be the same for every experiment. We used 1/16″ outer diameter (OD) PTFE tubing (Darwin Microfluidics, 1/32″ inner diameter [ID]) to connect all parts of the setup.

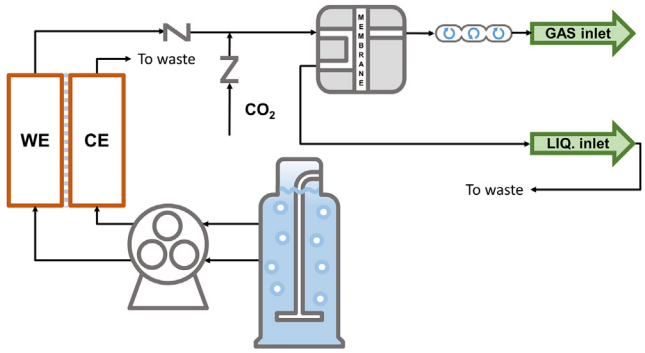

Figure 3. Schematic overview of the DEMS setup

CO_2 saturated electrolyte is pumped through the cell. The catholyte flows via a check valve through a tee-junction where it mixes with dry CO_2 gas. Afterward, the two phases are separated using a bubble trap. The separated gas flows through a static mixer into the gas inlet of the DEMS, while the liquid directed goes to the liquid inlet of the setup. CE, counter electrode; LIQ., liquid; WE, working electrode.

For reproducible and steady CO_2RR product detection, it is vital that the products are collected by the mass spectrometer in a manner corresponding with their rate of production inside the cell. However, if the cell outlet is directly connected to the DEMS inlet, the mass spectrum signal becomes unstable when bubbles start to form on the electrode and pass over the DEMS membrane after their release. This is in correspondence with Clark et al., who reported that as soon as bubbles were formed, the SD of the mass signal increased instantaneously by a factor of 100.[10] This observation can be explained by the vast difference in the density of gaseous products in the gas phase and dissolved in the electrolyte, as the product density in a bubble is much higher than in the saturated electrolyte. Therefore, when a released bubble passes over the DEMS inlet membrane, much more product passes through in a short period of time compared to when saturated electrolyte flows over the inlet of the DEMS. As a result, the amount of product passing the membrane will fluctuate greatly when the membrane is presented with an immiscible flow of bubbles and saturated electrolyte.

To stabilize the signal of the mass spectrometer, the electrolyte and bubbles exiting the flow cell need to be separated and enter the mass spectrometer simultaneously via two different inlets. However, simply separating bubbles from the saturated electrolyte is not enough. If both phases are immediately separated from each other after they exit the flow cell, then part of the formed gaseous products will enter the mass spectrometer from the gas phase, while the dissolved gaseous products in the electrolyte will enter from the liquid phase. Each of these phases has a different collection efficiency. As a result, the mass signal will no longer be linearly dependent on the product formation rate.[19] Therefore, all dissolved gaseous products need to be extracted from the liquid electrolyte. In that case, all the gaseous products will enter the mass spectrometer in the gas phase while all the liquid products will enter the mass spectrometer dissolved in the electrolyte. Each do so simultaneously through their respective inlets, which will be referred to as the gas and liquid inlet, respectively. Drawings and pictures of the gas and liquid inlet can be found in section S.3 of the supplemental information.

To adhere to these design criteria, the catholyte is pumped through a PEEK tee-union, where it mixes with dry CO_2 gas that is delivered by a CO_2 mass flow controller (EL-FLOW Select). A schematic drawing of this can be found in Figure 4. Due to the absence of products in the CO_2 gas, dissolved gaseous products are

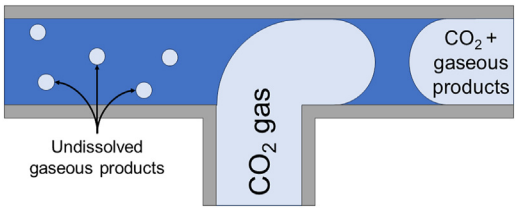

Figure 4. Schematic drawing of the tee-junction where the catholyte is mixed with a dry flow of CO_2 gas

Both phases travel together down a stainless-steel tube, during which dissolved gaseous products are drawn from the electrolyte into the gas slugs.

withdrawn from the liquid phase into the gas slugs while traveling down the tube. Before both the gas and electrolyte inlet, a microfluidic check valve prevents the fluid flowing the wrong way (Masterflex One-Way, Avantor and IDEX, inline check valve). A microfluidic check valve was chosen for the liquid stream to minimize bubble holdup. A 4.5-cm-long 100-μm ID PEEK tube (VWR) was used to insert the gas into the tee-junction, while a 4.5-cm-long 0.010-in. ID PEEK (VWR) tube was used for the catholyte to create a stable Taylor flow regime to enhance the mass transfer of gaseous products from the electrolyte to the gas phase. After the tee-union, both electrolyte and gas flow together through a 15-cm-long stainless-steel tube (1/8 in. OD, 1/16 in. ID, Swagelok) in a Taylor flow regime. A rigid material is used here to stabilize the flow rate of the Taylor flow. The gas and liquid are subsequently separated from each other using a commercial bubble trap (Large PEEK bubble remover, Elveflow) with a hydrophobic membrane.

From here, the separated phases are sent to their respective DEMS inlet. However, the product concentration that flows into the gas inlet still remains intermittent even when the product formation is constant, as bubbles containing gaseous products will still leave the flow cell at irregular intervals. To smooth the concentration gradient at the gas inlet over time, a static mixer was placed between the bubble trap and gas inlet to mix the gas stream before it enters the mass spectrometer. The design of the mixer was based on a series of three small spherical mixing chambers of about 3 cm in diameter with small 3-mm holes to separate them. At the end of the mixer two PEEK Frits (2 μm, IDEX) were placed to increase the pressure inside the mixer. Figure 5 shows a schematic drawing of the static mixer. In the liquid inlet, a PTFE membrane (20 nm pore size, Hangzhou Cobetter Filtration Equipment) is used to separate the dissolved liquid products from the electrolyte.

Including the static mixer will result in a more spread-out residence time distribution that has to be taken into account to correctly link the production rate in the cell to the corresponding mass peak signal. To determine the residence time distribution of the setup, a step input experiment was performed by performing chronopotentiometry experiments at −20 mA for 15 min in a CO_2-sparged 0.1 M $KHCO_3$ electrolyte using a Pt working electrode.[20] Since Pt is relatively inactive for CO_2 reduction, the only obtained product is hydrogen, and the mass peak 2 m/e can be used to follow the retention time of hydrogen in the setup. The results can be found in Figure 6. Here, the influence of the static mixer can be clearly seen. Even though hydrogen is being produced in the cell at t = 0, there is a clear delay until the produced hydrogen is detected by the mass spectrometer. In the first minute, there is no hydrogen detection due to the tubing between the cell and the mass spectrometer. Once the gas reaches the static mixer, the concentration starts to increase steadily. After roughly 7 min, the concentration stabilizes and the production in the cell matches the collection of the mass spectrometer. When the chronopotentiometry is stopped at t = 15 min, the process happens in reverse: first, there seems to be no change for about a minute, and then the concentration at the inlet begins to drop until it reaches the

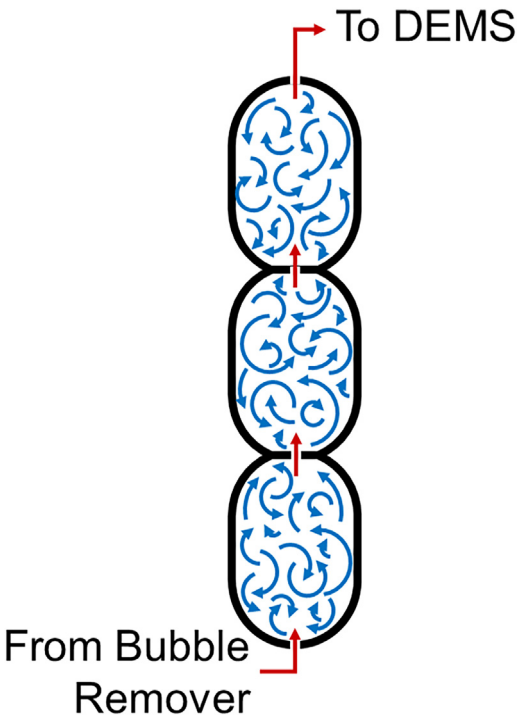

Figure 5. Schematic drawing of the static mixer

The incoming gas flow is mixed over the direction of the flow through the 3 metal bulbs that are stacked on top of one another. The static mixer is added to the setup to improve the homogeneity in product concentration in the gas flow before it enters the DEMS.

background value. The rate of production matches what the mass spectrometer measures only 7 min after an experiment has started. Then, about 1 min after the experiment ends, the measured products start to decline. Therefore, to make sure that the production rate accurately quantifies products, only measurements within such a measurement window were taken into account. In practice this means that instead of sweeping between two potentials, a series of chronoamperometry measurements is performed of 15 min each. For each measured potential, measurement data acquired between 7.8 and 16.3 min after the start of the chronoamperometry were taken into account to quantify products.

Product detection and quantification

The setup must be able to quantify the most common CO_2 reduction products—hydrogen, CO, formic acid, methane, ethylene, methanol, ethanol, allyl-alcohol, and 1-propanol.[21,22] Carboxylic acids, such as formic or acetic acid, are present as ions in the neutral electrolyte and are therefore unable to pass the PTFE membrane at the inlet of the mass spectrometer. Therefore, they cannot be detected by the DEMS and are omitted from the calibration. Instead, these products were quantified using HPLC. CO suffers from a lot of background signal as its mass spectrum overlaps with CO_2 (12, 16, and 28 m/e) and N_2 (28 m/e). To minimize the background noise from CO_2, mass 28 m/e is measured at a lower electron energy (19.5 eV), which is the dissociative ionization barrier for CO^+ from CO_2.[23] As a result, the electron current for this mass peak signal had to be lowered to 50 μA to avoid filament failure. To remove background signal coming from air-derived nitrogen as much as possible, the back pressure of the scroll pump is supplied with Ar at 1.15 bar_g and a flow rate of 0.4 L/min. Moreover, since PTFE tubing is not leak tight under vacuum conditions, air will leak into the setup and create background from air that leaks into the setup as a result of the vacuum. To circumvent this, all tubing between the gas outlet of the bubble trap and the gas inlet of the DEMS is

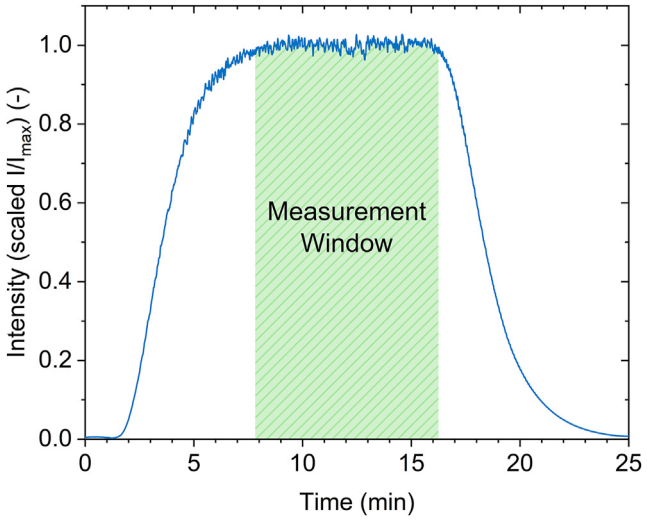

Figure 6. Step response function of the DEMS setup

The intensity was rescaled to the maximal measured intensity to show that all formed hydrogen was collected by the DEMS setup. The measurement window is shaded in green.

made from stainless steel and has Swagelok fittings. Due to the similar structure and small mass of the main products, there is much overlap between mass peaks of the different products. Moreover, mass peaks cannot be used for the quantification of products if they are obstructed by too much background signal from other species, such as CO_2, water, air, or Ar. Therefore, there is a limited number of mass peaks that can be used to detect and quantify the formed products. To optimize the settings of the mass spectrometer (electron current and secondary electron multiplier [SEM] voltage), ethanol is calibrated by flowing a series of increasingly diluted standards from 5 mM to 50 μM through the mass spectrometer using different settings (see section S.4 of the supplemental information). The limit of detection for each mass peak is estimated by dividing the SD by the slope of the obtained calibration coefficient for each mass peak signal. The lowest overall limit of detection was obtained at an electron current of 500 μA, an electron energy at 70 eV, and SEM voltage of 870 V. At these settings, 11 mass peaks could be used to quantify products with a limit of detection of 5 μM: 2, 15, 26, 27, 28, 30, 31, 41, 57, 58, and 59 m/e. Other mass peaks that should give a mass peak signal, such as 29 m/e, have too much background noise to be used for product quantification. As mentioned earlier, mass 28 m/e is measured at an electron energy of 19.5 eV and an electron current of 50 μA. A mass peak of 2 m/e is also measured at these settings to prevent overload at high production rates. Most of these mass peaks have overlapping contributions from multiple reduction products and must be deconvoluted.

Mass peak deconvolution and product quantification

For the mass peak deconvolution, the measured mass peak signals Y and the relative product concentrations X are assumed to satisfy the following linear model:

$$Y = \mu + BX + E \qquad \text{(Equation 2)}$$

where Y is an 11-dimensional vector containing the 11 measured mass peak signals, B is an 11 × 8-dimensional matrix that contains the coefficients, X is an 8-dimensional vector that contains the concentrations of the 8 products to be calibrated, μ is an

11-dimensional vector that contains the background signals of each of the 11 mass peak signals, and E is an 11-dimensional random vector representing the measurement error. The quantification of products is done in two major parts. The first part is a calibration step in which the matrix B is estimated on the basis of observed combinations of mass peak signals and relative gas concentrations. The second part is the quantification step, in which the vector X of gas concentrations is determined from newly measured mass peak signals and background signals.

Each liquid product is calibrated separately with aqueous solutions of each analyte in concentrations between 5 mM and 50 μM, while the gas products are simultaneously calibrated using calibration mixtures with concentrations between 8,000 ppm and 50 ppm of analytes balanced in CO_2. Since the units of concentration of the gaseous and liquid products are not the same, they are converted to their corresponding molar production rate in mol/s. The values of the coefficients are first estimated through calibration. If there was no linear correlation between the product and mass peak according to National Institute of Standards and Technology reference spectra,[24] then the coefficient was set to zero. On the basis of $n = 26$ observed pairs $(\overline{Y}_i, X_i)$ of (averaged) mass peak signals and relative gas concentrations, the remaining non-zero elements in the coefficient matrix are estimated by means of constrained least-squares minimization, conditional on having non-negative coefficients. Each $\overline{Y}_i$ is the average of multiple observed mass peak signals with the same gas concentration X_i. More details about the minimization and the resulting coefficient matrix $\widehat{B}$ can be found in supplemental information section S.5.

To quantify the products during a chronoamperometry measurement, new mass peak signals $Y_1^*, \ldots, Y_m^*$ are obtained during the measurement window (see Figure 6) and are averaged, such that a vector $\overline{Y}^* = (\overline{y}_1^*, \ldots, \overline{y}_{11}^*)$ with 11 averaged mass peak signals is obtained:

$$\overline{y}_j^* = \frac{1}{m}\sum_{k=1}^{m} y_{k,j}^*, j = 1, \ldots, 11 \qquad \text{(Equation 3)}$$

Finally, the background varied from day to day and must therefore be measured separately at the beginning of each experiment or calibration series. To get an estimate of the background value, the cell is run at open circuit potential for 30 min before the chronoamperometry measurements. The mass peaks $Y_1^{BG}, \ldots, Y_p^{BG}$ measured during these 30 min are averaged to obtain a new estimate for the vector of background signals $\widehat{\mu}^* = (\widehat{\mu}_1^*, \ldots, \widehat{\mu}_{11}^*)$ in the same way that mass peak signals obtained during the measurement window were averaged before:

$$\widehat{\mu}_j^* = \frac{1}{p}\sum_{k=1}^{p} \mu_{k,j}^{BG}, j = 1, \ldots, 11 \qquad \text{(Equation 4)}$$

Here, p denotes the number of mass peak signal measurements that were obtained during the 30 min of open circuit potential. To extract the concentrations from the new mass peak signals $Y_1^*, \ldots, Y_m^*$, we assume that they satisfy the linear model in Equation 2. Before the quantification step, a qualitative identification step is taken to determine which products could be present. Each compound of interest has one or several major mass peak signals that must be significantly higher than the baseline $(\widehat{\mu}^*)$ when the compound is present. To identify which peaks were significantly higher than their baseline value, for each mass peak signal $(j = 1, \ldots, 11)$ a two-sample t test is performed for the groups of background signals $y_{1,j}^{BG}, \ldots, y_{p,j}^{BG}$

and mass peak signals $y^*_{1,j}, \ldots, y^*_{m,j}$. To this end, the value of the test statistic is computed as:

$$t_j = \frac{\overline{y}^*_j - \widehat{\mu}^*_j}{\sqrt{\frac{s^2_{1,j}}{m} + \frac{s^2_{2,j}}{p}}} \quad \text{(Equation 5)}$$

where $s^2_{1,j}$ and $s^2_{2,j}$ are the sample variances of the mass peak signals $y^*_{1,j}, \ldots, y^*_{m,j}$ and background signals $y^{BG}_{1,j}, \ldots, y^{BG}_{p,j}$, respectively. They are calculated using the following formulas:

$$s^2_{1,j} = \frac{1}{m-1} \sum_{k=1}^{m} \left(y^*_{k,j} - \overline{y}^*_j \right)^2 \quad \text{(Equation 6)}$$

$$s^2_{2,j} = \frac{1}{p-1} \sum_{k=1}^{p} \left(y^{BG}_{k,j} - \widehat{\mu}^*_j \right)^2 \quad \text{(Equation 7)}$$

If all identifying mass peaks of a compound pass the t test with a one-tailed alpha of 0.05, the compound is produced and can be quantified. Otherwise, it is not likely that the compound was produced, and its concentration is set to zero during the quantification. The selected identifying mass peaks for each of the compounds can be found in the supplemental information (section S.5). After the identification step, the concentrations are computed by means of constrained least-squares minimization:

$$\min_{\substack{0 < x_s < UB \\ s = 1,\ldots,8}} \| \overline{Y}^* - \widehat{\mu} - \widehat{B}X \|^2 \quad \text{(Equation 8)}$$

During the least-squares minimization, each coordinate x_s of X is constrained to be between zero and an upper bound UB_s. The upper boundary is determined by first calculating a 95% confidence upper bound for $\sum_{s=1}^{8} \beta_{j,s} x_s$, for each mass peak ($j = 1, \ldots, 11$) separately, by means of the formula:

$$\mathrm{CB}_j = \overline{Y}_j^{\,*} - \widehat{\mu}^*_j + z_{0.95} \sqrt{\frac{s^2_{1,j}}{m} + \frac{s^2_{2,j}}{p}} \quad \text{(Equation 9)}$$

where $z_{0.95}$ denotes the 95th percentile of the standard normal distribution. An upper bound for x_s can then be determined by setting all other elements of X to zero and plugin the estimate for $\beta_{j,s}$. If a compound has multiple identifying mass peaks, then the smallest upper bound is taken. This leads to the formula:

$$\mathrm{UB} = \min_{j = 1,\ldots,11} \frac{\mathrm{CB}_j}{\widehat{\beta}_{j,s}}, s = 1, \ldots, 8 \quad \text{(Equation 10)}$$

Rapid electrocatalyst screening

To demonstrate the ability of the setup to quantify all major CO_2RR reaction products, a series of 15-min chronoamperometry measurements are performed with decreasing potential from −0.6 V vs. RHE to −1.3 V vs. RHE on both a polycrystalline Ag and Cu electrode in triplicate. Polycrystalline Ag and Cu are chosen as benchmarks in accordance with the benchmark set by Bell and co-workers.[25] The results can be found in Figure 7. The trends of products over the potential range fit well with other literature sources for both polycrystalline Ag[26] and Cu.[22] For Ag, the current partial densities (Figure S2) are comparable to reported values in the literature (~3 mA/cm^2 for CO at higher potentials, see section S.6 of the supplemental information) and follow similar trendlines over the measured potential range[26]: At low

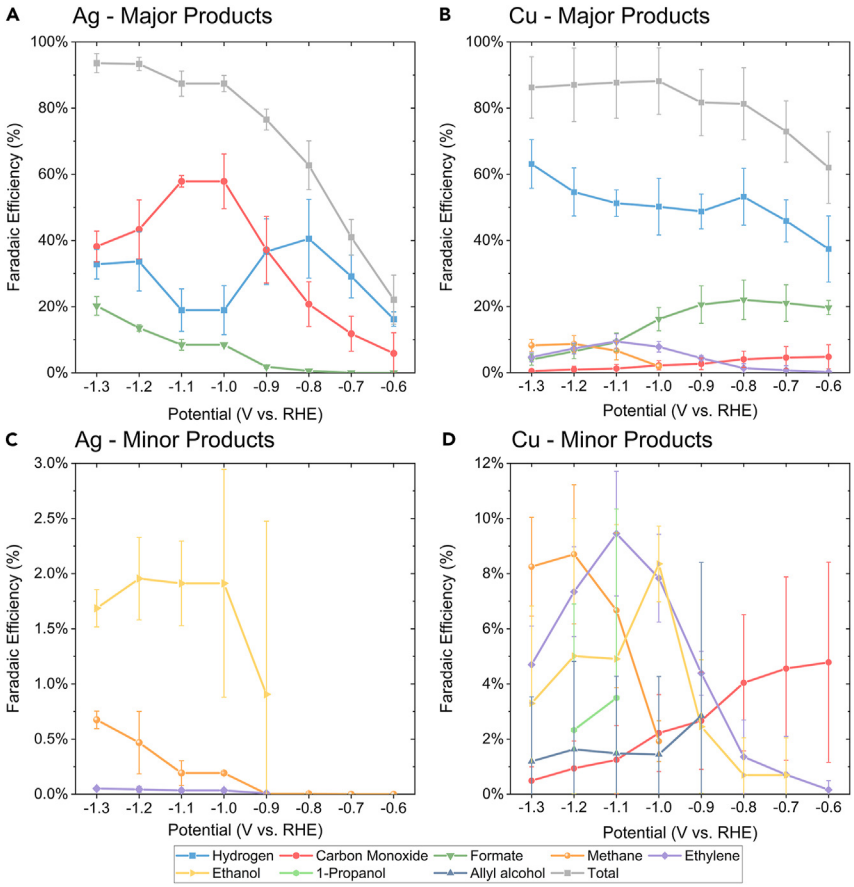

Figure 7. Faradic efficiencies of detected CO_2 reduction products

Products are given as a function of potential for both Ag (A and C) and Cu (B and D) electrodes divided into major and minor products, respectively. The error bars indicate the standard deviation between three repetitions of the same experiment around their average.

potentials, hydrogen production is dominant, but CO production slowly picks up, and around −0.9 V vs. RHE, the catalyst is more selective toward CO. However, at higher potentials, the production of CO stagnates, and hydrogen production picks up. Meanwhile, formate production slowly rises from lower to higher potentials and at higher potentials further reduced products such as ethanol and methane are detected. On Cu, the product current densities follow the same trendlines as in the literature[21,22]; the selectivity of formic acid and CO decreases from low to high potentials. At intermediate potentials, ethylene selectivity increases, but at higher potentials this decreases as well, similar to the alcohol selectivity. Finally, methane production becomes more prevalent toward higher potentials. Overall, this measurement confirms that the designed setup and analysis procedure is able to rapidly and accurately quantify the product distribution of CO_2RR electrocatalysts.

At low overpotentials, and therefore low production rates, the faradic efficiency balance could not be closed to 100%. This is due to a relatively greater influence of the value of the predetermined background signal (μ) at concentrations close to the lower limit of detection. Additionally, if there are remaining sources contributing to the background in the setup (residual nitrogen), then this will result in a higher estimate of the background signal. These background noises will diminish over time,

and at the start of the first chronoamperometry, the actual background signal will be less, leading to an underestimation of the production rate. Especially at low activity, these slight underestimations have a relatively greater influence. Additionally, some data points have larger SDs, especially the alcohols and CO. This is a result of the identifying step taken during the product deconvolution procedure. These products have a mass peak with a relatively large background noise (28 and 31 m/e for CO and alcohols, respectively) and small coefficients compared to the other products such as hydrogen, methane, and ethylene. As a result, the resulting mass peak signals of 28 and 31 m/e when CO or alcohols are produced will not always be significantly higher than the background signal, and the production rate will be set at 0. This results in much larger SDs between the different product runs.

The quantification could be sped up even further by shortening the governing residence time distribution of the setup. The residence time distribution itself is limited by the gas holdup in the cell, and the intermittent, discrete manner gas products leave the cell in the form of bubbles. Therefore, some mixing is required to obtain some level of continuous product effluent. To shorten the residence time, the PEEK cell could be pretreated by ozone, making the cell more hydrophilic and thereby reducing the gas holdup.[11] Also, the setup could be slightly redesigned to work under high pressure conditions. Under high pressure, the solubility of gasses in the electrolyte is enhanced, limiting the number of bubbles that are formed and increasing the mass transfer rate to the electrode surface.

Conclusion

An improved DEMS setup was designed that enables the simultaneous quantification of gaseous and liquid products during the electrochemical reduction of CO_2 significantly faster than conventional analytical techniques and without the need for additional *ex situ* measurements. Alternatively, the setup could be used for probing the long-term stability of catalysts by extending the time of the chronoamperometry measurement. The DEMS setup was validated by comparing the catalytic activity of a polycrystalline Cu and Ag electrode against benchmarks from the literature. Currently, the setup is able to quantify the production rate of most of the major CO_2 reduction products CO, methane, ethylene, methanol, ethanol, 1-propanol, and allyl alcohol. Therefore, to the best of our knowledge, it is the first DEMS setup that is able to simultaneously quantify CO and liquid products without the need for additional measurements.

To further improve the current setup, the residence time distribution could be shortened, or the detection limit could be lowered. To shorten the residence time distribution of the setup, the bubble holdup over the cell needs to decrease. One could treat the PEEK cell with ozone, similar to Clark et al.,[11] but this needs specialized setups like an ozone generator. Alternatively, the cell could be redesigned to work under high pressure. At elevated pressure, the solubility of the gas products increases, and bubble formation is prevented. To reduce the product detection limit, the background noise of the mass spectrometer signal can be reduced by optimizing the vacuum setup and regularly baking out the setup or by increasing the area of the PTFE membrane to the liquid inlet. A larger area would increase the flow of products into the mass spectrometer and thereby increase the detectability of the mass spectrometer to liquid products.

Compared to conventional research in H cells, where the researcher needs to accumulate liquid products for about 1 h, the designed setup is about 4 times faster in determining the catalytic response of a new electrocatalyst over a wide potential

range. Therefore, the DEMS setup can significantly speed up electrocatalyst development by enabling the testing of different catalyst materials in a short period of time. Additionally, it enables researchers to widen the number of reaction conditions they can test—for instance, using wider potential ranges or different electrolytes. As the hydrodynamics of the cell were quantified and successfully modeled, different hydrodynamic conditions can be used to probe reaction kinetics. Finally, unlike previously reported DEMS setups, the researcher is not limited to a single-cell design and the setup can be easily adapted to different cell designs.

EXPERIMENTAL PROCEDURES

Resource availability

Lead contact

Further information and requests for resources should be directed to and will be fulfilled by the lead contact, Dr. Ruud Kortlever (r.kortlever@tudelft.nl).

Materials availability

This study did not generate new materials.

Data and code availability

Any additional information required to reanalyze the data reported in this paper is available from the lead contact upon request.

Materials and chemicals

All solutions were prepared using ultrapure water (Millipore Milli-Q gradient A10 system, 18 MΩ cm) and reagents of high purity. Electrolytes were prepared using $KHCO_3$ (≥99.95%, Sigma-Aldrich), $K_3Fe(CN)_6 \cdot H_2O$ (99.9%, Sigma Aldrich), and $K_4Fe(CN)_6$ (99.9%, Sigma Aldrich). Polycrystalline silver foils (25 × 25 × 1 mm, 99.995%) were purchased from MaTecK GmbH, polycrystalline Cu foils (25 × 25 × 1 mm, 99.99%) were obtained from Sigma-Aldrich, while glassy carbon electrodes (25 × 25 × 1 mm) were purchased from HTW (Sigradur, polished). As the counter electrode, either a Pt foil (MaTeck Gmbh, 25 × 25 × 0.1 mm, 99.995%) or a glassy carbon electrode (HTW, Sigradur, polished) was used. For the calibration of the liquid products, methanol (≥99.9% Sigma-Aldrich), ethanol (≥99.8%, Sigma-Aldrich), 1-propanol (≥99.9% Sigma-Aldrich), and allyl-alcohol (≥99% Sigma-Aldrich) were used to make dilution series.

Electrochemical measurements

All electrochemical experiments were performed using a Biologic SP-200 potentiostat, using an RE-6 Ag/AgCl reference electrode (BASi).

Electrode preparation

Prior to every measurement, the polycrystalline Ag and Cu foils were polished by hand using 3-μm and 1-μm diamond paste (DP-floc, Struers) and a microfiber cloth (DP-floc, Struers) for a couple of minutes to ensure that contaminants were removed from the surface. After each polishing step, the electrode was washed using ultrapure water and subsequently dried using compressed nitrogen or Ar. After mechanical polishing, the Cu foil was electropolished twice in 85 vol/vol % H_3PO_4 (aq) solution (Sigma-Aldrich). In short, a two-electrode setup was used with the Cu foil as the working electrode and a carbon rod as the counter electrode. Cu tape (AT528, Advance Tapes) was used to hold up the Cu foil while both electrodes were immersed in a 100-mL beaker containing the electrolyte. A potential difference of 2.1 V was applied between the two electrodes for 3 min. After electropolishing, the Cu foil was washed with ultrapure water and dried using compressed Ar. Glassy

carbon electrodes were first cleaned using acetone to remove any leftover glue on the surface from the tape used in the previous experiments. Next, the electrode was ultrasonicated using ultrapure water for at least 15 min and manually polished for a couple of minutes using undiluted alumina paste (DP-floc, Struers) and a microfiber cloth (DP-floc, Struers). After another washing step with ultrapure water, the electrode was ultrasonicated in ultrapure water for 15 min to remove any residual alumina particles from the surface. Subsequently, the electrodes were ultrasonicated for 15 min in a 20 vol % HNO_3 (aq) solution (prepared with 70 vol % HNO_3 from Sigma-Aldrich) to make sure all leftover alumina dissolved from the electrode surface. Then, the electrode was washed and ultrasonicated for at least 15 min using ultrapure water to ensure all acid was removed from the electrode. Finally, the electrodes were dried using compressed nitrogen or Ar. Prior to each experiment, the Pt counter electrode was polished by hand using 3-μm diamond paste and a microfiber cloth (DP-floc, Struers) for about 1–2 min to make sure any contaminants were removed from the surface. Next, it was washed with ultrapure water and flame annealed until the surface glowed red-hot.

Ferro-/ferricyanide experiments

The ferro-/ferricyanide redox couple was used to determine the hydrodynamics of the cell. A buffer of 0.1 M $KHCO_3$ (99.95%, Sigma Aldrich) + 5 mM $K_3Fe(CN)_6 \cdot H_2O$ (99.9%, Sigma Aldrich) + 5 mM $K_4Fe(CN)_6$ (99.9%, Sigma Aldrich) was flowed through the cell, using glassy carbon as both the working and counter electrodes.[27] Furthermore, Ar was bubbled through the electrolyte to remove any dissolved oxygen, to prevent ferrocyanide oxidation.[28] Lastly, all experiments were performed in the dark to prevent photolysis of the cyanide complexes through photodissociation under UV light, leading to cyanide formation.[29] Linear sweep voltammetry was performed from open circuit potential to +0.6 V vs. E_{oc} at a sweep rate of 1 mV/s and maintaining different flow rates. The sweep rate was kept low to limit the contribution of double-layer charging. Cell resistances could not be determined using potentiostatic electrochemical impedance spectroscopy (PEIS) since at any potential faradaic reactions occur. Therefore, these results are shown without ohmic drop compensation.

Formate quantification

Because ions cannot pass the DEMS membrane, it was not possible to quantify the formate production at each potential. Instead, formate production was quantified using HPLC. Following the obtained residence time distribution, the electrolyte exiting the liquid DEMS inlet was collected 7 min after the chronoamperometry measurement started. The concentration of formate was measured by injection 100 μL into the HPLC (Agilent Technologies 1260 Infinity) to quantify the formed liquid products. The HPLC was calibrated with a dilution series in the range of 0.01–5 mM of formic acid (95%, Sigma-Aldrich). The flow rate of the eluent (1 mM H_2SO_4 (aq)) was set to 0.6 mL/min, and the measurement ran for 1 h. The HPLC used two Aminex HPX-87H columns (BioRad) in series heated to 60°C. A refractive index detector was used for the detection of products.

Mass spectrometer settings

MS was performed on a Hiden HPR40 dissolved-species mass spectrometer. All incoming species were first ionized and subsequently accelerated with a voltage of 3 V and an electron current of 500 μA. Finally, all cations were detected by an SEM, which was set at a voltage of 870 V. The electron current and SEM voltage were optimized to maximize the signal-to-noise ratio of liquid products (see the section Product detection and quantification).

Product calibration

For the gaseous products, five standard concentration bottles were used (Linde). The concentration of analytes in these bottles ranged from 50 to 100, 1,000, 3,000 and 8,000 ppm. The bottles were balanced with CO_2 and the flow rate used for calibration was 2 ml_n/min. Additionally, the background values of each mass peak were measured by flowing pure CO_2 through the setup. At startup or after changing the bottle, the signal was first stabilized for at least 3 h. Each liquid product was calibrated by flowing a series of increasingly diluted standards from 5 mM to 1 mM, 500 μM, 100 μM, and 50 μM. Each standard was prepared using ultrapure water and was pumped through the liquid inlet with a flow rate of 1 mL/min for 30 min before measurements were taken. After each dilution series had ended, ultrapure water was pumped through the system to obtain the background noise of each signal.

SUPPLEMENTAL INFORMATION

Supplemental information can be found online at https://doi.org/10.1016/j.checat.2024.101065.

ACKNOWLEDGMENTS

The authors thank Jim Melling from HIDEN for his never-wavering help during the initial troubleshooting of the DEMS setup.

AUTHOR CONTRIBUTIONS

Conceptualization, D.v.d.B. and R.K. Data curation, D.v.d.B. Data analysis, D.v.d.B. and R.K. Formal analysis, D.v.d.B. Investigation, D.v.d.B. Writing – original draft, D.v.d.B. Writing – mass peak deconvolution and product quantification, D.v.d.B. and H.P.L. Supervision, R.K. Funding acquisition, R.K.

DECLARATION OF INTERESTS

The authors declare no competing interests.

Received: February 8, 2024
Revised: June 13, 2024
Accepted: June 27, 2024
Published: July 23, 2024

REFERENCES

1. De Luna, P., Hahn, C., Higgins, D., Jaffer, S.A., Jaramillo, T.F., and Sargent, E.H. (2019). What would it take for renewably powered electrosynthesis to displace petrochemical processes? Science *364*, 1–9. https://doi.org/10.1126/science.aav350.

2. Shin, H., Hansen, K.U., and Jiao, F. (2021). Techno-economic assessment of low-temperature carbon dioxide electrolysis. Nat. Sustain. *4*, 911–919. https://doi.org/10.1038/s41893-021-00739-x.

3. Olah, G.A., Prakash, G.S., and Goeppert, A. (2011). Anthropogenic chemical carbon cycle for a sustainable future. J. Am. Chem. Soc. *133*, 12881–12898. https://doi.org/10.1021/ja202642y.

4. Trivedi, D. (2021). Electrochemical Reduction of Carbon Dioxide: Product Analysis and Cell Design (Lancaster University).

5. Wolter, O., and Heitbaum, J. (1984). The Adsorption of CO on a Porous Pt-Electrode in Sulfuric Acid Studied by DEMS. Ber. Bunsenges. Phys. Chem. *88*, 6–10. https://doi.org/10.1002/bbpc.19840880104.

6. Wolter, O., and Heitbaum, J. (1984). Differential electrochemical mass spectroscopy (DEMS)—a new method for the study of electrode processes. Ber. Bunsenges. Phys. Chem. *88*, 2–6. https://doi.org/10.1002/bbpc.19840880103.

7. Gao, Y., Tsuji, H., Hattori, H., and Kita, H. (1994). New on-line mass spectrometer system designed for platinum-single crystal electrode and electroreduction of acetylene. J. Electroanal. Chem. *372*, 195–200. https://doi.org/10.1016/0022-0728(93)03291-V.

8. Jambunathan, K., and Hillier, A. (2003). Measuring electrocatalytic activity on a local scale with scanning differential electrochemical mass spectrometry. J. Electrochem. Soc. *150*, E312. https://doi.org/10.1149/1.1570823.

9. Wonders, A.H., Housmans, T.H.M., Rosca, V., and Koper, M.T.M. (2006). On-line mass spectrometry system for measurements at single-crystal electrodes in hanging meniscus configuration. J. Appl. Electrochem. *36*, 1215–1221. https://doi.org/10.1007/s10800-006-9173-4.

10. Clark, E.L., and Bell, A.T. (2018). Direct observation of the local reaction environment during the electrochemical reduction of CO2. J. Am. Chem. Soc. *140*, 7012–7020. https://doi.org/10.1021/jacs.8b04058.

11. Clark, E.L., Singh, M.R., Kwon, Y., and Bell, A.T. (2015). Differential Electrochemical Mass Spectrometer Cell Design for Online Quantification of Products Produced during

Electrochemical Reduction of CO_2. Anal. Chem. *87*, 8013–8020. https://doi.org/10.1021/acs.analchem.5b02080.

12. Rao, V., Cremers, C., Stimming, U., Cao, L., Sun, S., Yan, S., Sun, G., and Xin, Q. (2007). Electro-oxidation of ethanol at gas diffusion electrodes a DEMS study. J. Electrochem. Soc. *154*, B1138. https://doi.org/10.1149/1.2777108.

13. Silva, W.O., Queiroz, A.C., Paganin, V.A., and Lima, F.H.B. (2018). Faradaic efficiency of ethanol oxidation to CO2 at metallic nanoparticle/short-side-chain PFSA solid-state electrolyte interfaces investigated by on-line DEMS. J. Electroanal. Chem. *824*, 99–107. https://doi.org/10.1016/j.jelechem.2018.07.035.

14. Bazán, J.C., and Arvia, A.J. (1965). The diffusion of ferro-and ferricyanide ions in aqueous solutions of sodium hydroxide. Electrochim. Acta *10*, 1025–1032. https://doi.org/10.1016/0013-4686(65)80014-7.

15. van Male, P., de Croon, M.H.J.M., Tiggelaar, R.M., van den Berg, A., and Schouten, J.C. (2004). Heat and mass transfer in a square microchannel with asymmetric heating. Int. J. Heat Mass Transf. *47*, 87–99. https://doi.org/10.1016/S0017-9310(03)00401-0.

16. Scherson, D.A., Tolmachev, Y.V., Wang, Z., Wang, J., and Palencsar, A. (2008). Extensions of the Koutecky–Levich equation to channel electrodes. Electrochem. Solid State Lett. *11*, F1. https://doi.org/10.1149/1.2818649.

17. Lobaccaro, P., Singh, M.R., Clark, E.L., Kwon, Y., Bell, A.T., and Ager, J.W. (2016). Effects of temperature and gas–liquid mass transfer on the operation of small electrochemical cells for the quantitative evaluation of CO2 reduction electrocatalysts. Phys. Chem. Chem. Phys. *18*, 26777–26785. https://doi.org/10.1039/C6CP05287H.

18. van den Berg, D., Izelaar, B., Fu, S., and Kortlever, R. (2024). The effect of surface conditions on the electrochemical CO2 reduction performance of bimetallic AuPd electrocatalysts. Catal. Sci. Technol. *14*, 555–561. https://doi.org/10.1039/D3CY01411H.

19. Bondue, C.J., and Koper, M.T.M. (2020). A DEMS approach for the direct detection of CO formed during electrochemical CO2 reduction. J. Electroanal. Chem. *875*, 113842. https://doi.org/10.1016/j.jelechem.2020.113842.

20. Fogler, H.S., and Brown, L. (2006). Elements of Chemical Reaction Engineering (Pearson).

21. Asperti, S., Hendrikx, R., Gonzalez-Garcia, Y., and Kortlever, R. (2022). Benchmarking the electrochemical CO2 reduction on polycrystalline copper foils: The importance of microstructure versus applied potential. ChemCatChem *14*, e202200540. https://doi.org/10.1002/cctc.202200540.

22. Kuhl, K.P., Cave, E.R., Abram, D.N., and Jaramillo, T.F. (2012). New insights into the electrochemical reduction of carbon dioxide on metallic copper surfaces. Energy Environ. Sci. *5*, 7050–7059. https://doi.org/10.1039/C2EE21234J.

23. Kronebusch, P.L., and Berkowitz, J. (1976). Photodissociative ionization in the 21–41 eV region: O2, N2, CO, NO, CO2, H2O, NH3 and CH4. Int. J. Mass Spectrom. Ion Phys. *22*, 283–306. https://doi.org/10.1016/0020-7381(76)80088-5.

24. NIST (2023). NIST Standard Reference Database 69 (NIST Chemistry WebBook). https://doi.org/10.18434/T4D303.

25. Clark, E.L., Resasco, J., Landers, A., Lin, J., Chung, L.-T., Walton, A., Hahn, C., Jaramillo, T.F., and Bell, A.T. (2018). Standards and protocols for data acquisition and reporting for studies of the electrochemical reduction of carbon dioxide. ACS Catal. *8*, 6560–6570. https://doi.org/10.1021/acscatal.8b01340.

26. Hatsukade, T., Kuhl, K.P., Cave, E.R., Abram, D.N., and Jaramillo, T.F. (2014). Insights into the electrocatalytic reduction of CO_2 on metallic silver surfaces. Phys. Chem. Chem. Phys. *16*, 13814–13819. https://doi.org/10.1039/C4CP00692E.

27. Blaedel, W., and Schieffer, G. (1977). A hydrodynamic voltammetric study of the ferricyanide/ferrocyanide system with convective electrodes of platinum, gold, glassy carbon, carbon film, and boron carbide. J. Electroanal. Chem. Interfacial Electrochem. *80*, 259–271. https://doi.org/10.1016/S0022-0728(77)80048-X.

28. Sutey, A., and Knudsen, J. (1967). Effect of Dissolved Oxygen on Redox Method for Measurement of Mass Transfer Coefficients. Ind. Eng. Chem. Fund. *6*, 132–139. https://doi.org/10.1021/i160021a023.

29. Arellano, C.A.P., and Martínez, S.S. (2010). Effects of pH on the degradation of aqueous ferricyanide by photolysis and photocatalysis under solar radiation. Sol. Energy Mater. Sol. Cells *94*, 327–332. https://doi.org/10.1016/j.solmat.2009.10.008.